

Article

Power Transformer's Electrostatic Ring Optimization Based on ANSYS Parametric Design Language and Response Surface Methodology

Gang Liu ^{1,*} , Danhui Hou ¹, Xiaojun Zhao ¹, Dongwei Yuan ¹, Lin Li ² and Youliang Sun ³

¹ Hebei Provincial Key Laboratory of Power Transmission Equipment Security Defense, North China Electric Power University, Baoding 071003, China; 15668259098@163.com (D.H.); 158748295@163.com (X.Z.); ydw2046@163.com (D.Y.)

² State Key Laboratory of Alternate Electrical Power System with Renewable Energy Sources, North China Electric Power University, Beijing 102206, China; lilin@ncepu.edu.cn

³ Shandong Power Equipment Co., Ltd., Jinan 250022, China; youliang.s@163.com

* Correspondence: liugang@ncepu.edu.cn

Received: 17 September 2019; Accepted: 10 October 2019; Published: 12 October 2019



Abstract: In this paper, in view of the low efficiency of the traditional finite element method (FEM), which has been widely used in the insulation design of power transformers, the response surface methodology (RSM) is proposed to optimize the insulation structure of a power transformer electrostatic ring. Firstly, the power transformer model was built using the ANSYS parametric design language (APDL) to realize the automatic pre-processing of numerical calculation. Then with the objective of reducing the maximum electric field intensity, the Taguchi method was used to select the parameters that have a greater impact on the maximum electric field intensity, by which the subsequent optimization process could be effectively simplified. The test points were constructed by the central composite design (CCD) and a response surface model was established by the mutual calls of MATLAB and ANSYS. Finally, the variance analysis, diagnostic analysis, and significance test of regression were carried out to obtain the final response surface model. By comparing the result of RSM with that of FEM, we can find that the results obtained by the two methods are consistent and the maximum electric field strength is obviously reduced. The RSM is more systematic and convincing, which improves the optimization efficiency and provides a reliable and fast way for the optimization of power transformers.

Keywords: power transformer; response surface methodology (RSM); ANSYS parametric design language (APDL); electric field analysis; electrostatic ring optimization

1. Introduction

As the main device of power systems, the power transformer is essential to the safe and reliable operation of the whole electrical network [1]. The insulation structure determines the electric field distribution; thus, the optimization of the main insulation structure is of great importance to ensure the safe and stable operation of the power transformer [2,3]. With the increase of voltage levels, more and more attention has been paid to the electrical insulation problem of the power transformer. However, the insulation structure of a transformer is particularly complex, which makes the electric field distribution non-uniform. Therefore, to confirm the rationality and reliability of the main insulation structure of the transformer, it is necessary to test, calculate, and analyze the electric field distribution [4].

In engineering applications, electric field analysis methods can be divided into two types, the analytical methods and the numerical methods. A few simple problems may be solved by the analytic method; but in the majority of cases, an analytical method simply does not exist or it is extremely difficult to obtain. As a numerical method, the FEM (finite element method) has been applied

in the electric field calculation [5–7]. In the electrostatic ring structure optimization [8], the traditional finite element method (FEM) was used to analyze the influence of each variable on the electric field intensity and summarize its changing rule through several specific points. The FEM generally adopted the inference method [8,9], and the optimal values of the parameters were obtained by summarizing the changing law of each variable. Although it is possible to get the result, it cannot prove that the final result is the optimal solution, and it needs to constantly modify the model parameters for modeling analysis, which increases the calculation time.

In addition to the FEM, the structure optimization methods roughly fall into two types. One is to establish the function expression between the optimization objective and the variables by using sensitivity analysis methods [10]. Sometimes the selection of step length is involved in the sensitivity analysis methods and the accuracy cannot be guaranteed. Moreover, the sensitivity formulas are difficult to derive, and the process is rather complicated [11]. When the analytical expression for the relationship between the optimization variables and optimization objectives cannot be found, the other type of methods, the global optimization methods, or the response surface methodology (RSM) combined with FEM can be used for the optimization design. Global optimization methods such as the genetic algorithm [12–16] and the particle swarm optimization algorithm [8,17–19] need to call a large number of modeling and optimization programs repeatedly, which significantly affect the efficiency of optimization. Most importantly, without appropriate fitness functions the local search ability may become worse and the search efficiency may be reduced.

The RSM constructs an approximate function expression between the objective function and variables, and visualizes the objective function that is originally implicit. The repeated modeling and simulation can be avoided; thereby, the efficiency of the optimization can be significantly improved [20]. As a mathematical and statistical optimization method [21,22], the RSM has been applied in many aspects. References [23] and [24] combined the RSM with the genetic algorithm and indicated that this method could reduce the number of experiments and solve the problem of fitness function selection. Reference [25] used the RSM to optimize the armature structure, and proved that this method had high feasibility, which provided an effective method for armature structure improvement. References [26–28] posed the methods for the optimization of an oil-immersed transformer cooling system and improved the design of the permanent magnet motor using RSM. In Reference [29], the RSM was employed to optimize the structure of the motor and the experiment on the prototype was carried out to verify the efficiency and reliability of the RSM. Reference [30] proposed a method by combining the RSM with the geometric feature charge simulated method to get the electric field; by using this method, the workload could be reduced and the computing time could be shortened as well. In addition, the RSM has been successfully applied in the mechanism of brake squeal [31], biochemistry [32], medicine [33], ships [34], machine design [35], and other fields.

According to the research above, the RSM demonstrates the ability to deal with many optimization problems with good speed and convenience on the premise of ensuring accuracy and efficiency. However, there is no relevant research on its application to the electrostatic ring structure optimization design of the power transformer.

In this paper, the RSM was applied to optimize the electrostatic ring structure of a 500 kV power transformer. The power transformer model was built with ANSYS parametric design language (APDL) [36,37] and the response surface model was constructed according to the optimization parameters selected by the Taguchi method [38,39]. Then, the fitting degree and prediction ability of the response surface model were analyzed to get the optimal result. Furthermore, we compared the optimization result with that of traditional FEM, and the accuracy and validity of the RSM were proved.

2. Finite Element Model and Research Method

2.1. Calculation Model

The calculation model of a 500 kV power transformer is shown in Figure 1 and the values of the initial parameters are listed in Table 1.

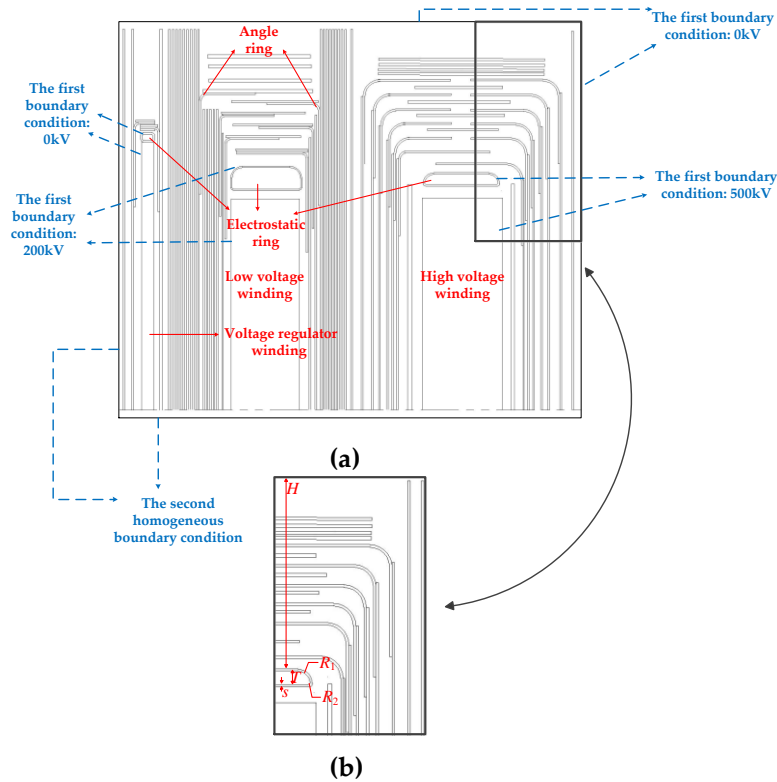


Figure 1. Calculation model of 500kV power transformer insulation structure. (a) Integral structure; and (b) partial structure.

Table 1. Initial parameter values.

Parameters	Physical Meanings	Initial Values
R_1	Upper arc radius of the electrostatic ring	18 mm
R_2	Lower arc radius of the electrostatic ring	8 mm
T	Thickness of the electrostatic ring	26 mm
H	Distance from the upper surface of the electrostatic ring to the iron yoke	274 mm
S	Thickness of the insulating layer	4 mm
W	Starting position of the first arc	48 mm

The boundary value problem of the electrostatic field can be expressed by Equation (1).

$$\begin{cases} -\nabla \cdot \varepsilon \nabla \varphi = \rho, & \varphi \in \Omega; \\ \varphi|_{\Gamma_1} = 5 \times 10^5, & \varphi|_{\Gamma_2} = 2 \times 10^5; \\ \varphi|_{\Gamma_3} = 0; \\ \frac{\partial \varphi}{\partial n}|_{\Gamma_{4,5}} = 0. \end{cases} \quad (1)$$

where ε is the dielectric constant; φ is the electric scalar potential of the electrostatic field; Ω is the whole computational domain; Γ_1 is the high voltage winding boundary; Γ_2 is the low voltage winding

boundary; Γ_3 is the regulating winding, the upper, and the right boundary; and $\Gamma_{4,5}$ are the left and lower boundary, respectively.

The APDL is applied to realize automatic pre-processing as follows: (1) The relative dielectric constants of oil and pressboard were 2.2 and 4.5, respectively; (2) the voltage applied on the high voltage winding was 500 kV (Γ_1), the low voltage winding was 200kV (Γ_2), and the voltage regulating winding and the upper and the right boundary were 0kV (Γ_3). These are the first kind of boundary conditions and (3) the left and lower boundary are the second kind of homogeneous boundary conditions ($\Gamma_{4,5}$). In addition, the boundary conditions of Figure 1b were interpolated based on the results of Figure 1a.

The computer processor we used had an Intel(R) Core(TM) i5-7500 with 8.00 GB of memory. After modeling, meshing, applying boundary conditions, and solving by APDL, the electric field intensity nephogram of the initial structure is shown in Figure 2. By analyzing the initial insulation structure of the power transformer, it can be found that the maximum electric field intensity appeared at the upper right corner of the electrostatic ring. Therefore, we try to reduce the maximum electric field intensity by changing the structure parameters related to the electrostatic ring.

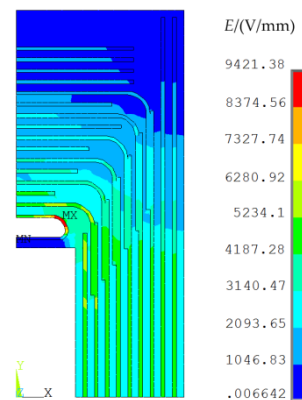


Figure 2. Electric field intensity distribution of the initial structure of a 500kV power transformer main insulation.

2.2. Taguchi Method

In the optimization experiments, the selection of the parameter that has no influence on the optimization result as a variable will not only increase the workload, but will also affect the accuracy of the optimization result. Therefore, the Taguchi method was employed to eliminate the irrelevant variables and select the parameters which have great influence on the maximum electric field intensity [40,41]. Then the response surface experiments were carried out with these filtered parameters, by which the optimization efficiency can be significantly improved.

The Taguchi method designs the horizontal combination of each parameter by establishing an orthogonal table, carries on an orthogonal experiment to calculate the proportion of the influence of each parameter on the optimization target, and filters the parameters according to the proportion. Each parameter that needs to be optimized usually takes three values in the range of change, which is called the impact factor.

2.3. RSM

The response surface model is also called the response surface function and the regression equation [42,43]. A proper function can make the approximation more precise and the design space more suitable for wider use. The quadratic polynomials can describe the real function and ensure that the model is as simple as possible with fewer undetermined coefficients. Its expression can be written as

$$\bar{y} = \beta_0 + \sum_{j=1}^n \beta_j x_j + \sum_{j=1}^n \beta_{jj} x_j^2 + \sum_{i=1}^n \sum_{j=i}^n \beta_{ij} x_i x_j, \tag{2}$$

where \tilde{y} is the objective function; $\beta_0, \beta_j, \beta_{jj},$ and β_{ij} are the polynomial coefficients; x_j is the j th experimental variable; and n is the number of experimental variables. Assuming that k times tests are needed to obtain the response surface model, Equation (2) can be expressed in the following matrix form:

$$\begin{pmatrix} y_1 \\ y_2 \\ \vdots \\ y_k \end{pmatrix} = \begin{pmatrix} 1 & x_{11} & \cdots & x_{1n} & x_{11}^2 & \cdots & x_{1n}^2 & x_{11}x_{12} & \cdots & x_{1n}x_{1n-1} \\ 1 & x_{21} & \cdots & x_{2n} & x_{21}^2 & \cdots & x_{2n}^2 & x_{21}x_{22} & \cdots & x_{2n}x_{2n-1} \\ \vdots & \vdots & \ddots & \vdots & \vdots & \ddots & \vdots & \vdots & \ddots & \vdots \\ 1 & x_{k1} & \cdots & x_{kn} & x_{k1}^2 & \cdots & x_{kn}^2 & x_{k1}x_{k2} & \cdots & x_{kn}x_{kn-1} \end{pmatrix} \cdot \left\{ \beta_0 \ \beta_1 \ \cdots \ \beta_n \ \beta_{11} \ \cdots \ \beta_{nn} \ \beta_{12} \ \cdots \ \beta_{nm-1} \right\}^T + \left\{ \mu_1 \ \mu_2 \ \cdots \ \mu_k \right\}^T \quad (3)$$

or

$$y = X\beta + \mu, \quad (4)$$

where μ is the error of y . The polynomial coefficients are obtained according to Equation (5) by using the least squares principle to minimize the sum of the squares of the errors.

$$\beta = (X^T X)^{-1} X^T y. \quad (5)$$

2.4. Central Composite Design (CCD)

The fitting accuracy of the RSM depends largely on the distribution of sample points in the design space. The CCD method follows specific rules when selecting the sample points [44–46]. According to the traditional method, when three variables and five levels are selected for experiments, at least 125(5³) experiments are needed. The CCD can minimize the number of experiments on the premise of good accuracy.

Figure 3 shows the distribution of sample points, taking three variables as an example [29]. Where $\alpha = 2^{n/4}$; (0,0,0) is the center point; $(\pm 1, \pm 1, \pm 1)$ is the cubic point; and $(\pm \alpha, 0, 0), (0, \pm \alpha, 0),$ and $(0, 0, \pm \alpha)$ are the axial points.

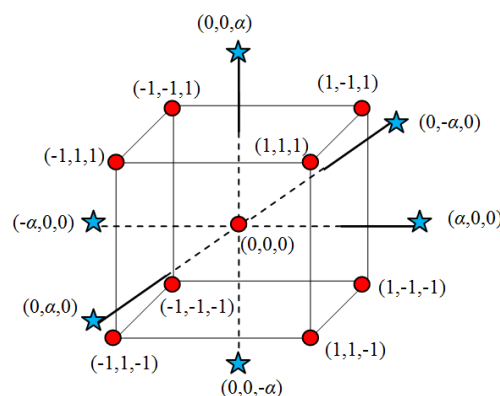


Figure 3. Distribution of three variables’ central composite design test points.

2.5. Test for Significance of Regression

A test which is usually used to verify the overall applicability of the model and the significance of regression is called null hypothesis [21,47], as follows:

$$H_0: \beta_1 = \beta_2 = \dots = \beta_n = 0,$$

$$H_1: \beta_j \neq 0 \text{ for at least one } j.$$

The value H_0 means that the variables have the same effect on the response value, and the error is only caused by the selection of the sample points. The rejection of H_0 indicates that at least one of the variables has a significant contribution to the model, that is, the model is reasonable. In addition,

the p -value approach, which reflects the probability of the H_0 , can be used to test the null hypothesis. If the p -value is less than 0.05, the null hypothesis is rejected, that is, the H_0 is invalid.

The value R^2 is the determination coefficient and R^2_{adj} is the adjusted R^2 . The closer their values are to 1, the better is the fitting effect of the model.

3. Experimental Process and Analysis

As can be seen in Section 2.1, the maximum electric field intensity emerged at the upper right corner of the electrostatic ring. Therefore, we can select the parameters related to the electrostatic ring as the variables to optimize. The structure and parameters of the electrostatic ring are shown in Figure 4.

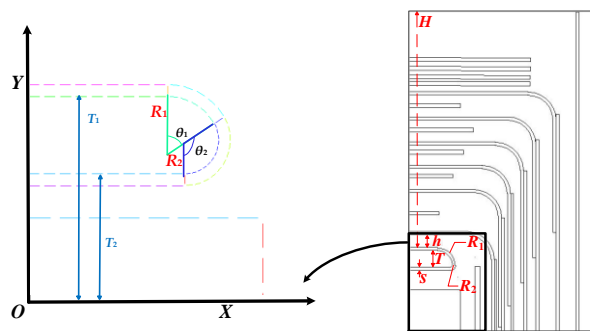


Figure 4. Structure and parameters of the electrostatic ring.

Due to the existence of the pressboard, for easy analysis, H is simplified as h , the distance from the top surface of the electrostatic ring (without insulation layer) to the first pressboard above the electrostatic ring. The relationship between the two arcs of the electrostatic ring can be expressed by Equation (6).

$$\begin{cases} \theta_1 + \theta_2 = 180^\circ \\ y_1 = T_1 - R_1 \\ R_2 = \frac{(y_1 + R_1 \cdot \cos \theta_1 - T_2)}{1 + \cos \theta_1} \\ x_2 = x_1 + (R_1 - R_2) \cdot \sin \theta_1 \\ y_2 = y_1 + (R_1 - R_2) \cdot \cos \theta_1 \end{cases} \quad (6)$$

Among them, the coordinates of the center of the two arcs are (x_1, y_1) and (x_2, y_2) . Values T_1 and T_2 are the ordinate values of the upper and lower surfaces of the electrostatic ring (excluding the insulating layer). As can be seen from the above equation, R_2 and θ_2 can be derived from R_1 and θ_1 . Therefore, the four optimization variables $R_1, \theta_1, R_2,$ and θ_2 can be simplified into two variables, namely R_1 and θ_1 .

The optimization process is demonstrated in Figure 5.

3.1. Taguchi Experiment

Through the above analysis, the Taguchi experiment was carried out with $R_1, \theta_1, h, s,$ and w as variables to be optimized. Taking the median values of the variables on both sides and their adjacent values as the impact factors, the impact factors of the optimized parameters are listed in Table 2.

Table 2. Parameters to be optimized and impact factors.

Parameters	R_1/mm	$\theta_1/^\circ$	h/mm	s/mm	w/mm
impact factor 1	10	52.5	12.5	2.75	42.5
impact factor 2	14	75	15	3.5	45
impact factor 3	18	97.5	17.5	4.25	47.5

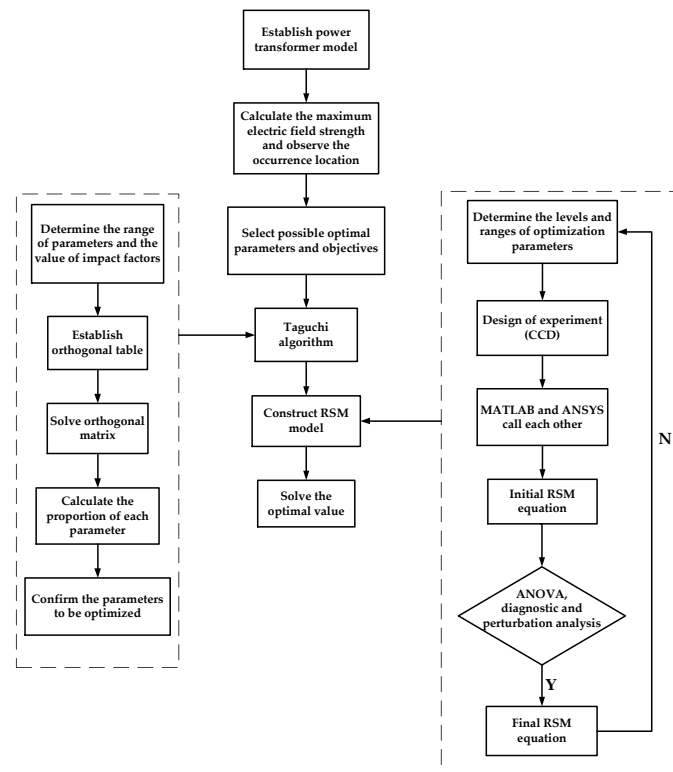


Figure 5. Flowchart of insulation structure optimization of power transformer based on RSM.

The orthogonal table $L_9(3^5)$ is obtained by the Taguchi method, where L represents an orthogonal matrix; 9 stands for the number of trials; 3 is the number of times each variable is taken, and 5 symbolizes the number of optimization parameters. According to the orthogonal table, the maximum electric field intensity can be achieved by the mutual call between MATLAB and ANSYS, as shown in the Table 3.

Table 3. Orthogonal matrix and results of $L_9(3^5)$.

Number of Experiments	R_1/mm	$\theta_1/^\circ$	h/mm	s/mm	w/mm	$E_{\text{max}}/(\text{V}/\text{mm})$
1	1	1	1	1	2	10385.95
2	1	2	2	2	1	9794.79
3	1	3	3	3	3	9615.61
4	2	1	2	3	1	9170.99
5	2	2	3	1	2	9928.34
6	2	3	1	2	3	9866.17
7	3	1	3	2	3	9681.51
8	3	2	1	3	2	9167.40
9	3	3	2	1	1	9559.65

From the results obtained by Table 3, the proportion of each parameter is calculated by Equation (7).

$$EE = 3 \sum_{i=1}^3 [m_{x_i}(E_i) - m(E)]^2, \tag{7}$$

where x_i represents $R_1, \theta_1, h, s,$ and w ; EE is the proportion of each optimization parameter; $m_{x_i}(E_i)$ is the average value of E_{max} under the i th impact factor of x ; and $m(E)$ is the average value of E_{max} . The proportion of each optimization parameter is listed in Table 4.

Table 4. Influence proportion of the optimized parameters on E_{max} .

Parameters	EE	Proportion (%)
R_1 /mm	325,162.8862	25.0
θ_1 /mm	20,294.4814	1.6
h /mm	140,533.0000	10.8
s /mm	655,163.7245	50.3
w /mm	160,650.0366	12.3
Total	1,301,804.1290	100

It can be seen from Table 5 that R_1 , h , s , and w have greater influence on the maximum electric field intensity, while θ_1 can be eliminated from the impact variables. The Taguchi method effectively reduced the workload of the numerical analysis of the subsequent response surface. In the following experiment, for the convenience of analysis, the electrostatic ring was divided into two arcs; both of them were 90 degrees. The values R_1 , h , s , and w were selected as experimental variables.

Table 5. Level of test factors by CCD.

Variables	Levels				
	$-\alpha$	-1	0	1	α
R_1	5	6	14	22	24
h	5	10	15	20	25
s	0.5	2	3.5	5	6.5
w	35	40	45	50	55

Note: The $-\alpha$ and α levels of R_1 are -1 and 27 , respectively, which exceed the range of variation and are appropriately adjusted.

3.2. Experimental Data

After determining the experimental variables, the appropriate range of values was selected for the response surface experiment. There are four optimization variables in this experiment, so $\alpha=2$. The design and combination of the experimental sample points were carried out by the CCD method, as shown in Table 5. Table 6 is the experimental data results of the sample points which were obtained by calling each other between ANSYS and MATLAB.

Table 6. Experimental data.

Run	Actual/mm				Coded				E_{max} /(V/mm)	Number of Elements	DOFs
	R_1	h	s	w	\bar{x}_1	\bar{x}_2	\bar{x}_3	\bar{x}_4			
1	6	10	5	40	-1	-1	1	-1	10,909.89	2074	3958
2	24	15	3.5	45	1.571	0	0	0	9154.23	2125	4038
3	13	15	0.5	45	0	0	-2	0	11,831.83	2528	4700
4	20	10	5	40	1	-1	1	-1	8599.39	2081	3967
5	6	20	5	50	-1	1	1	1	11,053.85	2080	3962
6	6	10	2	50	-1	-1	-1	1	12,416.88	2133	4047
7	13	15	3.5	45	0	0	0	0	9664.49	2090	3981
8	13	15	3.5	45	0	0	0	0	9664.49	2090	3981
9	20	20	5	50	1	1	1	1	8870.22	2080	3957
10	13	15	6.5	45	0	0	2	0	9328.45	2087	3983
11	13	5	3.5	45	0	-2	0	0	10,048.23	2131	4060
12	20	20	5	40	1	1	1	-1	8243.91	2082	3963
13	6	20	2	50	-1	1	-1	1	11,789.22	2140	4057
14	6	10	2	40	-1	-1	-1	-1	11,656.15	2128	4044
15	13	15	3.5	45	0	0	0	0	9664.49	2090	3981
16	13	25	3.5	45	0	2	0	0	9151.81	2129	4035
17	17	15	3.5	55	0	0	0	2	10,380.85	2088	3973
18	6	10	5	50	-1	-1	1	1	11,564.39	2076	3959

Table 6. Cont.

Run	Actual/mm				Coded				E_{max} /(V/mm)	Number of Elements	DOFs
	R_1	h	s	w	\bar{x}_1	\bar{x}_2	\bar{x}_3	\bar{x}_4			
19	20	20	2	50	1	1	-1	1	10,083.12	2153	4073
20	5	15	3.5	45	-1.413	0	0	0	11,879.20	2102	4004
21	13	15	3.5	45	0	0	0	0	9664.49	2090	3981
22	20	10	2	40	1	-1	-1	-1	9758.90	2137	4053
23	13	15	3.5	45	0	0	0	0	9664.49	2090	3981
24	20	10	2	50	1	-1	-1	1	10,391.28	2147	4006
25	20	10	5	50	1	-1	1	1	9179.16	2079	3961
26	6	20	5	40	-1	1	1	-1	10,354.56	2082	3970
27	13	15	3.5	45	0	0	0	0	9664.49	2090	3981
28	20	20	2	40	1	1	-1	-1	9314.94	2145	4064
29	13	15	3.5	35	0	0	0	-2	9077.65	2086	3977
30	6	20	2	40	-1	1	-1	-1	11,046.17	2131	4047

The last two columns of Table 6 are the number of elements and nodes (degrees of freedom) of the local finite element model in Figure 1b. According to statistics, it took only 61.8 seconds to complete the above 30 CCD experiments. Without the CCD method, 625 RSM experiments would be required. Thus, by using CCD method, the optimization efficiency was greatly improved.

Referring to the above data, the coefficients of the response surface model were obtained by Equation (5). We can get the initial response surface model from Table 7.

Table 7. Coefficients of RSM model.

Factor	df	Standard Error	95% CI Low	95% CI High	Coefficient Estimate
Intercept	1	54.99	9583.37	9817.79	12419.312
R_1	1	31.52	-1120.49	-986.12	-371.458
h	1	28.29	-290.01	-169.40	-55.687
s	1	28.29	-588.97	-468.36	-783.092
w	1	28.29	275.97	396.58	84.888
R_1h	1	34.65	-18.43	129.30	1.584
R_1s	1	34.65	-175.73	-28.00	-9.701
R_1w	1	34.65	-89.55	58.18	-0.448
hs	1	34.65	-57.65	90.08	2.162
hw	1	34.65	-60.77	86.95	0.524
sw	1	34.65	-95.39	52.33	-2.870
R_1^2	1	42.70	382.68	564.71	9.667
h^2	1	26.20	-90.83	20.87	-1.399
s^2	1	26.20	154.20	265.90	93.357
w^2	1	26.20	-58.52	53.18	-0.107

3.3. Analysis of Variance

The ANOVA table summarizes the results of the variance analysis, as shown in Table 8.

As shown in Table 8, the p -value of the regression model was less than 0.0001, which means that the choice of the quadratic polynomial model is reasonable, and the relationship between the maximum electric field intensity value, y , and the regression equation is extremely significant. Thus, the null hypothesis, H_0 , is not valid and can be rejected. The p -value of all linear terms were less than 0.0001, indicating that each variable in R_1 , h , s , and w is an extremely significant factor affecting the optimization objective. Except that the interaction between R_1 and s was significant, the p -value of each of the other two was greater than 0.05, demonstrating the interaction between the two has little effect on the response. The p -values of the quadratic terms R_1^2 and s^2 were less than 0.0001, and the significance was higher than the other two, which is an extremely significant factor. In addition, R_{adj}^2 is 0.9841, which is very close to 1. The model can explain 98.41% of the test changes and better reflect the

law of data changes with less experimental error and better fitting. Furthermore, from the confidence interval listed in Table 8, the significant items are also $R_1, h, s, w, R_1s, R_1^2,$ and $s^2,$ for the upper and lower bounds of their confidence intervals do not contain zero.

Table 8. Analysis of variance.

Source of Variation	Sum of Squares	Degrees of Freedom	Mean Square	F_0	p -Value	Significance
Regression	3.468×10^7	14	2.477×10^6	128.92	<0.0001	***
R_1	2.146×10^7	1	2.146×10^7	1116.64	<0.0001	***
h	1.266×10^6	1	1.266×10^6	65.91	<0.0001	***
s	6.708×10^6	1	6.708×10^6	349.10	<0.0001	***
w	2.714×10^6	1	2.714×10^6	141.25	<0.0001	***
R_1h	4.917×10^4	1	4.917×10^4	2.56	0.1305	
R_1s	1.660×10^5	1	1.660×10^5	8.64	0.0101	*
R_1w	3.936×10^3	1	3.936×10^3	0.20	0.6573	
hs	4.207×10^3	1	4.207×10^3	0.22	0.6466	
hw	2.741×10^3	1	2.741×10^3	0.14	0.7109	
sw	7.415×10^3	1	7.415×10^3	0.39	0.5438	
R_1^2	2.365×10^6	1	2.365×10^6	123.06	<0.0001	***
h^2	3.424×10^4	1	3.424×10^4	1.78	0.2018	
s^2	1.235×10^6	1	1.235×10^6	64.26	<0.0001	***
w^2	199.590	1	199.590	0.01	0.9202	
Lack of Fit	2.882×10^5	15	2.882×10^5			
Pure Error	0.000	5	0.000			
Total	3.497×10^7	29				

Note: *** Extremely significant; ** Very significant; * Significant

3.4. Diagnostic Analysis

To verify the applicability of the model, the diagnostic analysis was generally made by making the regression analysis and giving some diagnostic plots.

The design of the normal probability plot made the cumulative normal distribution a straight line. In Figure 6a, the points on the normal probability plot were approximately distributed in a straight line, which indicates the accuracy of the data for calculating the electric field intensity.

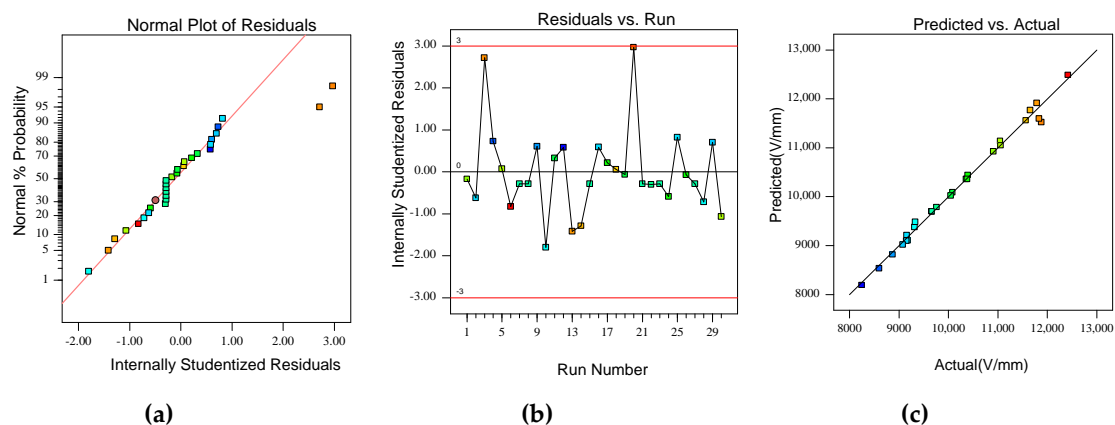


Figure 6. (a) Normal probability distribution of residuals; (b) residuals versus run; and (c) predicted values versus actual values.

As can be seen from the residuals versus run plot in Figure 6b, the residuals of runs were distributed within the prescribed appropriate range, which implies that choosing the quadratic polynomial as the response surface function is particularly suitable. In Figure 6c and Table 9, there was a good correlation

between the predicted value and the actual value, which indicates that the polynomial model has a good predictive ability. In a word, the response surface model adopted in this study is acceptable.

Table 9. Comparisons between predicted and actual values.

Run	Actual Values/(V/mm)	Predicted Values/(V/mm)
1	10,909.89	10,924.76
2	9154.23	9215.12
3	11,831.83	11,598.13
4	8599.39	8534.92
5	11,053.85	11,047.78
6	12,416.88	12,488.54
7	9664.49	9700.58
8	9664.49	9700.58
9	8870.22	8816.94
10	9328.45	9483.46
11	10,048.23	10,020.08
12	8243.91	8192.64
13	11,789.22	11,912.01
14	11,656.15	11,767.75
15	9664.49	9700.58
16	9151.81	9101.26
17	10,380.85	10,362.45
18	11,564.39	11,559.45
19	10,083.12	10,088.63
20	11,879.20	11,523.06
21	9664.49	9700.58
22	9758.90	9785.36
23	9664.49	9700.58
24	10,391.28	10,443.42
25	9179.16	9106.87
26	10,354.56	10,360.74
27	9664.49	9700.58
28	9314.94	9378.21
29	9077.65	9017.35
30	11,046.17	11,138.85

3.5. 3-D Response Surface Analysis

For a better demonstration of the influence of the interaction between two variables, the 3-D plots were adopted. If the interaction has a significant impact on the response surface, the variation of 3-D plot will be accordingly large.

Figure 7a shows that when R_1 and s interact, if we fix one of the variables and increase the other variable, the maximum electric field intensity will decrease. As can be seen from the trend of the surface graph, the maximum electric field intensity decreased faster with R_1 than with s , indicating that R_1 has a greater influence on the response value. Comparing Figure 7a with Figure 7b, the response surface of Figure 7b fluctuated slightly, which means that the change of the interaction term hw has no significant effect on the maximum electric field intensity. Similarly, hs and sw are not significant factors either.

As can be seen from Figure 7c,d, compared with s and w , the change of the maximum electric field intensity was larger with the change of R_1 . The maximum electric field intensity increases with the increase of w , which has negative effects on the model. Therefore, in the structural design process, a smaller starting position w should be selected as far as possible within a reasonable range. From the variation range of the two figures, the interactions between R_1 and h , R_1 , and w may be a significant factor affecting the maximum electric field intensity. However, since their p -values in Table 8 are little larger than 0.05, R_1h and R_1w can be considered insignificant factors.

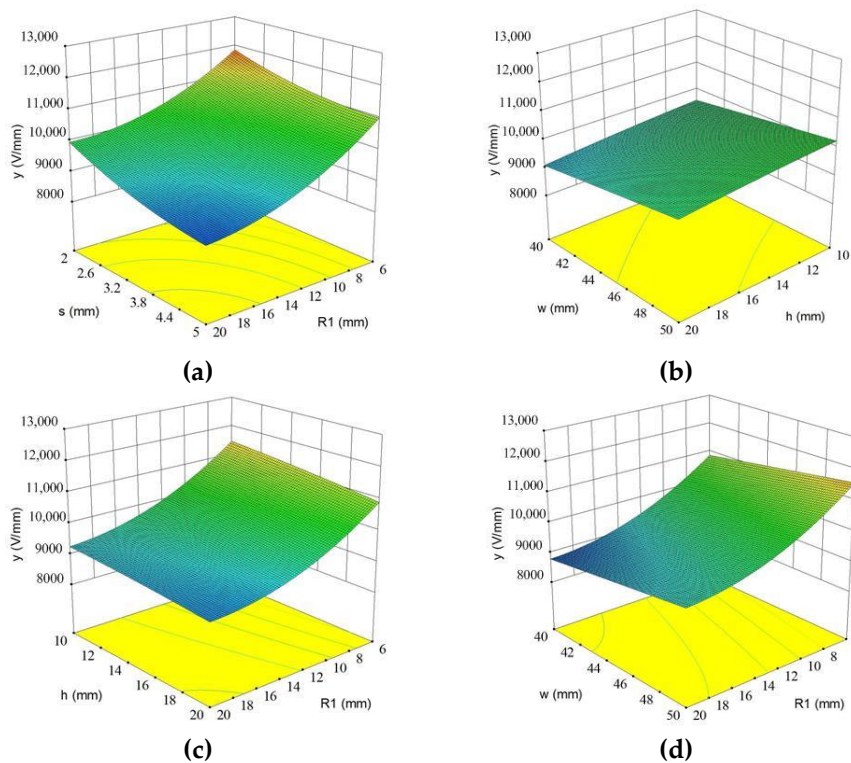


Figure 7. 3-D plot of the interaction between two variables: (a) R_1s , (b) hw , (c) R_1h , and (d) R_1w .

Through the above analysis, the insignificant factors, such as R_1h , R_1w , hs , hw , sw , h^2 , and w^2 , are removed, and the final response surface equation with a higher prediction ability is shown in Equation (8).

$$y = 12419.312 - 371.458 * R_1 - 55.687 * h - 783.092 * s + 84.888 * w - 9.701 * R_1 * s + 9.667 * R_1^2 + 93.357 * s^2 \tag{8}$$

4. Results and Discussion

It is an important goal of the response surface optimization to get the optimal results with the appropriate values assigned to each variable. Equation (8) is the quadratic response surface model with single objective optimization, which can be solved quickly by quadratic programming. By comparing the maximum electric field intensities on the electrostatic ring before and after optimization in Figure 8, the decrease of the maximum electric field intensity can be observed more intuitively. The result shows that the maximum electric field intensity has been significantly reduced.

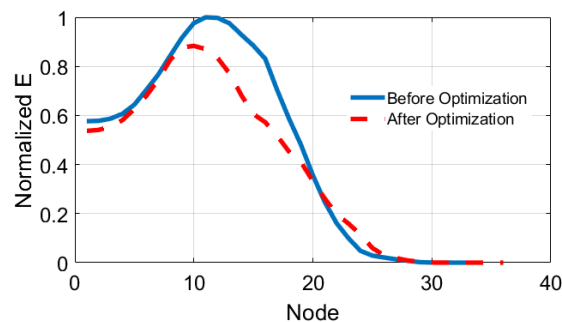


Figure 8. Comparison of electric field intensity of electrostatic ring before and after optimization.

In order to verify the validity of the RSM, we compared the result of RSM with that of traditional FEM. The FEM taking much time and requiring many experiments, to ensure the fairness of the experiment and save the calculation time, thirty experiments were carried out by using the FEM. As can be seen from Table 10, the results obtained by RSM and FEM were consistent, while the time the of RSM experiments was much less, which demonstrates the effectiveness of RSM and also shows the high optimization efficiency and good prediction ability of this method.

Table 10. Optimization results.

Before and After Optimization	Variables				E_{max} (V/mm)	Decline Rate (%)	Experimental Time(s)
	R_1 (mm)	h (mm)	s (mm)	w (mm)			
Before Optimization	18	15	4	48	9303.30	-	
FEM	22	20	5	40	8219.83	11.6	2400
RSM	22	20	5	40	8192.64	12.1	61.8

In Figure 9, a comparison of the variations of variables predicted by the FEM and those actually obtained by the RSM was made. It can be observed that the variations of variables in this paper are monotonic, so FEM can obtain the optimal results by inference in this special case. However, this method is no longer applicable when the variables are not monotonic. The RSM has a wider range for applications and the result obtained by it is more rigorous and convincing.

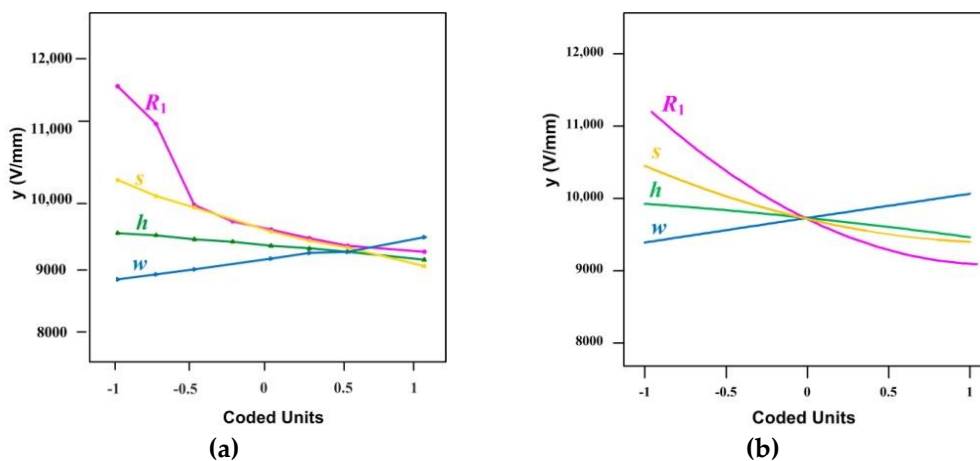


Figure 9. Comparison of optimization results: (a) FEM; (b) RSM.

5. Conclusions

In this paper, the response surface methodology, Taguchi method, and ANSYS parametric modeling language were combined to optimize the electrostatic ring of a 500 kV power transformer. The APDL extracted the maximum electric field intensity automatically and the mutual calls between MATLAB and ANSYS solved the problem of repeated manual modeling and meshing in traditional methods. To avoid the increased calculating workload of developing experiments aroused by irrelevant variables, the Taguchi method was utilized to filter the variables before making response surface experiments, by which the optimization process was effectively simplified. The experimental points were constructed by the experimental design method of CCD, and the response surface model was then obtained. In order to ensure the accuracy and predictability of the model, the response surface model was analyzed by ANOVA, diagnostic analysis, and the significance test of regression, and the final response surface equation was determined. Comparing the optimization results with the traditional finite element method, on the premise of ensuring accuracy, the proposed method in this paper has a higher optimization efficiency.

In general, the structure of the electrostatic ring is optimized more systematically and completely through the Taguchi method and response surface experiments. The feasibility and efficiency of this method were verified, which provides a new and more systematic, fast, and efficient way for the optimization of the transformer insulation structure.

Author Contributions: Conceptualization, G.L.; methodology, G.L., D.H., and D.Y.; software, G.L.; validation, X.Z.; formal analysis, Y.S.; investigation, X.Z.; resources, L.L.; data curation, D.Y.; writing—original draft preparation, D.H.; writing—review and editing, G.L.; visualization, D.H. and D.Y.; supervision and project administration, L.L.; funding acquisition, X.Z.

Funding: This work is supported in part by the National Key Research and Development Program of China (Grant No. 2017YFB0902703), in part by the National Natural Science Foundation of China under Grant 51407075, in part by Fundamental Research Funds for the Central Universities of China under Grant 2019MS076.

Conflicts of Interest: The authors declare no conflict of interest.

References

- Li, H.K.; Jing, Y.T.; Li, Y.; Li, L.N.; Han, F.X. Structure design and electromagnetic analysis of EHV double-body power transformer. *High Volt. Eng.* **2016**, *42*, 2322–2338.
- Amoiralis, E.I.; Tsili, M.A.; Georgilakis, P.S. The state of the art in engineering methods for transformer design and optimization: Asyrvey. *J. Optoelectron. Adv. Mater.* **2008**, *10*, 1149–1158.
- Hugo, R.I.; Xose, M.L.F.; Casimiro, A.M. A methodology for the optimized design of power transformer insulation system. *COMPEL Int. J. Comput. Math. Electr. Electron. Eng.* **2018**, *37*, 1002–1010.
- DiBarba, P.; Galdi, R.; Piovan, U.; Savini, A.; Consogno, G. Optimal shape design of a high-voltage test arrangement. *COMPEL Int. J. Comput. Math. Electr. Electron. Eng.* **2004**, *23*, 633–638. [[CrossRef](#)]
- Bramanti, A.; DiBarba, P.; Piovan, U.; Savini, A. Design optimization of transformer insulation. In *Electromagnetic Fields in Electrical Engineering*; Krawczyk, A., Wiak, S., Eds.; IOS Press: Amsterdam, The Netherlands, 2002; pp. 170–173.
- Anderson, O.W. Transformer leakage flux program based on the finite element method. *IEEE Trans. Power Appar. Syst.* **1973**, *PAS-92*, 682–689. [[CrossRef](#)]
- Amoiralis, E.I.; Georgilakis, P.S.; Tsili, M.A.; Kladas, A.G. Global transformer optimization method using evolutionary design and numerical field computation. *IEEE Trans. Magn.* **2009**, *45*, 1720–1723. [[CrossRef](#)]
- Wang, S.B. *Design of Main Insulation Structure of Power Transformer Based on Particle Swarm Optimization*; School of Mechanical Engineering Shenyang University of Technology: Shenyang, China, 2012.
- Han, L. *Numerical Analysis of Electric Field for the Insulation Structure of Winding End of Power Transformer*; Hebei University of Technology: Tianjin, China, 2013.
- Cui, X.; Zhang, G.Q. Sensitivity analysis and automatic design of electromagnetic parameters in power apparatuses. *Proc. Chin. Soc. Electr. Eng.* **2010**, *20*, 17–20.
- Infante, B.J.; Mota, S.C.M.; Mota, S.C.A.M. Sensitivity analysis and shape optimal design of axisymmetric shell structures. *Comput. Syst. Eng.* **1991**, *2*, 525–533.
- Yu, Q.J.; Wang, Z.J. Optimal graded insulation design of power transformer windings by genetic algorithms. *Proc. Chin. Soc. Electr. Eng.* **2000**, *20*, 21–24.
- Zhang, S.L.; Peng, Z.R. Nonlinear E-field simulation of converter transformer outlet and its structure optimization. *High Volt. Eng.* **2018**, *44*, 2048–2059.
- Deng, Q.H.; Shao, S.; Fu, L.; Luan, H.F.; Feng, Z.P. An integrated design and optimization approach for radial inflow turbines—Part II: Multidisciplinary optimization design. *Appl. Sci.* **2018**, *8*, 2030. [[CrossRef](#)]
- Gorni, D.; Visioli, A. Genetic algorithms based reference signal determination for temperature control of residential buildings. *Appl. Sci.* **2018**, *8*, 2129. [[CrossRef](#)]
- Sun, X.; Lai, L.F.; Chou, P.; Chen, L.R.; Wu, C.C. On GPU implementation of the island model genetic algorithm for solving the unequal area facility layout problem. *Appl. Sci.* **2018**, *8*, 1604. [[CrossRef](#)]
- Li, F.; Ren, X.C.; Luo, W.B.; Chen, X.W. Methodology for existing railway reconstruction with constrained optimization based on point cloud data. *Appl. Sci.* **2018**, *8*, 1782. [[CrossRef](#)]
- Liu, C.; Shen, Z.Z.; Gan, L.; Xu, L.Q.; Zhang, K.L.; Jin, T. The seepage and stability performance assessment of a new drainage system to increase the height of a tailings dam. *Appl. Sci.* **2018**, *8*, 1840. [[CrossRef](#)]

19. Reza, A.; Vahid, R.; Ebrahim, R. Gray box modeling of power transformer windings based on design geometry and particle swarm optimization algorithm. *IEEE Trans. Power Deliv.* **2018**, *33*, 2384–2393.
20. Sui, Y.K.; Yu, H.P. *Improvement of Response Methodology and Its Application to Engineering Optimization*; Science Press: Beijing, China, 2010; pp. 4–22.
21. Raymond, H.M.; Douglas, C.M.; Christine, M.A. *Response Surface Methodology: Process and Product Optimization Using Design Experiments*, 4th ed.; John Wiley & Sons: Hoboken, NJ, USA, 2016; pp. 1–307.
22. Hidemi, T.; Mitsuru, K.; Hidetoshi, I.; Monami, S. Interpolation of turbulent boundary layer profiles measured in flight using response surface methodology. *Appl. Sci.* **2018**, *8*, 2320.
23. Zhang, Y.F.; Xu, Y.L. Design of rotor structure of permanent magnet brushless motor for EV based on genetic algorithm and response surface method. *Micromotors* **2018**, *51*, 6–12.
24. Lou, D.M.; Zhao, C.Z.; Yu, H.Y.; Tan, P.Q.; Hu, Z.Y. Optimization of injection parameters for diesel engine during transient process based on response surface method and genetic algorithm. *Veh. Engine* **2017**, 45–50. [[CrossRef](#)]
25. Li, B.; Lu, J.Y.; Tan, S.; Li, Y.; Zhang, Y.S. Optimal method under the effect of multi-factor for C-shaped solid armature. *High Volt. Eng.* **2016**, *42*, 2060–2066.
26. Zhang, Y.P.; Ho, S.L.; Fu, W.N. Applying Response Surface Method to Oil-Immersed Transformer Cooling System for Design Optimization. *IEEE Trans. Magn.* **2018**, *54*, 8401705. [[CrossRef](#)]
27. Liu, X.Y.; Fu, W.N. A dynamic Dual-Response-Surface Methodology for Optimal Design of a Permanent-Magnet Motor Using Finite-Element Method. *IEEE Trans. Magn.* **2016**, *52*, 7204304. [[CrossRef](#)]
28. Pedram, A.; Ramon, B.P.; Mohammadreza, B. Global sizing optimisation using dual-level response surface method based on mixed-resolution central composite design for permanent magnet synchronous generators. *IET Electr. Power Appl.* **2018**, *12*, 684–692.
29. Li, Z.; Zhang, L.; Wang, Q.J.; Lun, Q.Q. Optimal design of structure parameters of three-DOF deflection type PM motor based on response surface methodology. *Trans. China Electrotech. Soc.* **2015**, *30*, 134–141.
30. Wu, Q.; Liu, X.M.; Zou, J.Y.; Yang, T. Numerical Solution and accuracy validation of electric field using response surface methodology and geometric feature charge simulation method. *High Volt. Eng.* **2018**, *44*, 2060–2066.
31. Chu, Z.; Zheng, F.; Liang, L.; Yan, H.; Kang, R. Parameter determination of a minimal model for brake squeal. *Appl. Sci.* **2018**, *8*, 37. [[CrossRef](#)]
32. He, Q.H.; Du, B.; Xu, B.J. Extraction optimization of phenolics and antioxidants from black goji berry by accelerated solvent extractor using response surface methodology. *Appl. Sci.* **2018**, *8*, 1905. [[CrossRef](#)]
33. Park, S.; Kang, H. Multivariate analysis of laser-induced tissue ablation: Ex vivo liver testing. *Appl. Sci.* **2017**, *7*, 974. [[CrossRef](#)]
34. Huang, C.Y.; Lin, Y.; Yu, Y.Y. Structural optimization of bulk carrier intensity deck by response surface methodology. *Chin. J. Ship Res.* **2012**, *7*, 46–50.
35. Chen, H.W.; Tian, C.; Peng, C.C.; Hu, B. Truss structure optimization design based on response surface method. *Mach. Des. Res.* **2016**, *32*, 48–52.
36. Gao, C.Y.; Zhang, X.Y.; Liu, X.Y.; Deng, Z.H.; Li, S.R. *ANSYS Parametric Programming Command and Example*; China Machine Press: Beijing, China, 2015.
37. Wang, G.Q. *Practical Engineering Numerical Simulation Technology and Its Practice on ANSYS*; Northwest Polytechnic University Press: Xi'an, China, 2001.
38. Vigneashwara, P.; Wahyu, C.; Tegoeh, T.; Gunasekaran, P. Predictive modelling and analysis of process parameters on materials removal characteristics in abrasive belt grinding process. *Appl. Sci.* **2017**, *7*, 363.
39. Ki, C.K.; Ju, L.; Hee, J.K.; Dae, H.K. Multiobjective optimal design for interior permanent magnet synchronous motor. *IEEE Trans. Magn.* **2009**, *45*, 1780–1783.
40. Lan, Z.Y.; Yang, X.Y.; Wang, F.Y.; Zheng, C.D. Application for optimal designing of sinusoidal interior permanent magnet synchronous motors by using the Taguchi method. *Trans. China Electrotech. Soc.* **2011**, *26*, 37–42.
41. Krzysztof, M.; Katarzyna, M.; Sebastian, B.; Jakub, B.; Alicja, T.; Marta, M.; Martyna, L.; Szymon, P.; Beata, G. Optimization of a culture medium using the Taguchi approach for the production of microorganisms active in odorous compound removal. *Appl. Sci.* **2017**, *7*, 756.
42. Nima, P.; Tang, X.W.; Yang, Q. Energy evaluation of triggering soil liquefaction based on the response surface method. *Appl. Sci.* **2019**, *9*, 694.

43. Cai, J.D.; Ye, R.; Chen, H.C. Aging diagnosis method of oil-paper insulation based on multiple parameter regression analysis of recovery voltage. *Trans. China Electrotech. Soc.* **2018**, *33*, 5080–5089.
44. Box, G.E.P.; Draper, N.R. *Empirical Model-Building and Response Surfaces*; Wiley: New York, NY, USA, 1987.
45. Leyla, R.; Hamid, N.; Ehsan, E.E.; Peter, W. Thermal management of a distribution transformer: An optimization study of the cooling system using CFD and response surface methodology. *Int.J. Electr. Power Energy Syst.* **2019**, *104*, 443–455.
46. Li, J.Y.; Liu, Z.T.; Jabbar, M.A.; Gao, X.K. Design Optimization for Cogging Torque Minimization Using Response Surface Methodology. *IEEE Trans. Magn.* **2004**, *40*, 1176–1179. [[CrossRef](#)]
47. Douglas, C.M.; Elizabeth, A.P.; Geoffrey, G.V. *Introduction to Linear Regression Analysis, 4th ed.*; China Machine Press: Beijing, China, 2017; pp. 1–116.



© 2019 by the authors. Licensee MDPI, Basel, Switzerland. This article is an open access article distributed under the terms and conditions of the Creative Commons Attribution (CC BY) license (<http://creativecommons.org/licenses/by/4.0/>).